



HAL
open science

Efficient Ray Traversal of Constrained Delaunay Tetrahedralization

Maxime Maria, Sébastien Horna, Lilian Aveneau

► **To cite this version:**

Maxime Maria, Sébastien Horna, Lilian Aveneau. Efficient Ray Traversal of Constrained Delaunay Tetrahedralization. 12th International Joint Conference on Computer Vision, Imaging and Computer Graphics Theory and Applications (VISIGRAPP 2017), Feb 2017, Porto, Portugal. pp.236-243. hal-01486575

HAL Id: hal-01486575

<https://hal.science/hal-01486575>

Submitted on 10 Mar 2017

HAL is a multi-disciplinary open access archive for the deposit and dissemination of scientific research documents, whether they are published or not. The documents may come from teaching and research institutions in France or abroad, or from public or private research centers.

L'archive ouverte pluridisciplinaire **HAL**, est destinée au dépôt et à la diffusion de documents scientifiques de niveau recherche, publiés ou non, émanant des établissements d'enseignement et de recherche français ou étrangers, des laboratoires publics ou privés.

Efficient Ray Traversal of Constrained Delaunay Tetrahedralization

Maxime Maria¹, Sébastien Horna¹ and Lilian Aveneau¹

¹University of Poitiers, XLIM, UMR 7252, Futuroscope Chasseneuil Cedex, Poitiers, France
{maxime.maria, sebastien.horna, lilian.aveneau}@univ-poitiers.fr

Keywords: Ray Tracing, Acceleration Structure, Constrained Delaunay Tetrahedralization

Abstract: Acceleration structures are mandatory for ray-tracing applications, allowing to cast a large number of rays per second. In 2008, Lagae and Dutré have proposed to use Constrained Delaunay Tetrahedralization (CDT) as an acceleration structure for ray tracing. Our experiments show that their traversal algorithm is not suitable for GPU applications, mainly due to arithmetic errors. This article proposes a new CDT traversal algorithm. This new algorithm is more efficient than the previous ones: it uses less arithmetic operations; it does not add extra thread divergence since it uses a fixed number of operation; at last, it is robust with 32-bits floats, contrary to the previous traversal algorithms. Hence, it is the first method usable both on CPU and GPU.

1 INTRODUCTION

Ray tracing is a widely used method in computer graphics, known for its capacity to simulate complex lighting effects to render high-quality realistic images. However, it is also recognized as time-consuming due to its high computational cost.

To speed up the process, many acceleration structures have been proposed in the literature. They are often based on a partition of Euclidean space or object space, like kd-tree (Bentley, 1975), BSP-tree, BVH (Rubin and Whitted, 1980; Kay and Kajiya, 1986) and regular grid (Fujimoto et al., 1986). A survey comparing all these structures can be found in (Havran, 2000). They can reach interactive rendering, *e.g.* exploiting ray coherency (Wald et al., 2001; Reshetov et al., 2005; Mahovsky and Wyvill, 2006) or GPU parallelization (Purcell et al., 2002; Foley and Sugerman, 2005; Günther et al., 2007; Aila and Laine, 2009; Kalojanov et al., 2011). Nevertheless, actually a lot of factors impact on traversal efficiency (scene layout, rendering algorithm, *etc.*).

A different sort of acceleration structures is the constrained convex space partition (CCSP), slightly studied up to then. A CCSP is a space partition into convex volumes respecting the scene geometry. (Fortune, 1999) introduces this concept by proposing a topological beam tracing using an acyclic convex subdivision respecting the scene obstacles, but using a hand-made structure. Recently, (Maria et al., 2017) present a CCSP dedicated to architectural environments, hence limiting its purpose. (Lagae and Dutré,

2008) propose to use a constrained Delaunay tetrahedralization (CDT), *i.e.* CCSP only made up of tetrahedra. However, our experiments show that their CDT traversal methods cannot run on GPU, due to numerical errors.

Using a particular tetrahedron representation, this paper proposes an efficient CDT traversal, having the following advantages:

- It is robust, since it does not cause any error due to numerical instability, either on CPU or on GPU.
- It requires less arithmetic operations and so it is inherently faster than previous solutions.
- It is adapted to parallel programming since it does not add extra thread divergence.

This article is organized as follows: Section 2 recapitulates previous CDT works. Section 3 presents our new CDT traversal. Section 4 discusses our experiments. Finally, Section 5 concludes this paper.

2 PREVIOUS WORKS ON CDT

This section first describes CDT, then it presents its construction from a geometric model, before focusing on former ray traversal methods.

2.1 CDT description

A Delaunay tetrahedralization of a set of points $X \in \mathbb{E}^3$ is a set of tetrahedra occupying the whole

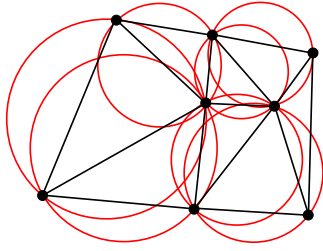


Figure 1: Delaunay triangulation: no vertex is inside a circumscribed circle.

space and respecting the Delaunay criterion (Delaunay, 1934): a tetrahedron T , defined by four vertices $V \subset X$, is a Delaunay tetrahedron if it exists a circumscribed sphere S of T such as no point of $X \setminus \{V\}$ is inside S . Figure 1 illustrates this concept in 2D. Delaunay tetrahedralization is “constrained” if it respects the scene geometry. In other words, all the geometric primitives are necessarily merged with the faces of the tetrahedra making up the partition.

Three kinds of CDT exist: usual constrained Delaunay tetrahedralization (Chew, 1989), conforming Delaunay tetrahedralization (Edelsbrunner and Tan, 1992) and quality Delaunay tetrahedralization (Shewchuk, 1998). In ray tracing context, (Lagae and Dutré, 2008) proved that quality Delaunay tetrahedralization is the most efficient to traverse.

2.2 CDT construction

CDT cannot be built from every geometric models. A necessary but sufficient condition is that the model is a piecewise linear complex (PLC) (Miller et al., 1996). In 3D, any non empty intersection between two faces of a PLC must correspond to either a shared edge or vertex. In other words, there is no self-intersection (Figure 2). In computer graphics, a scene is generally represented as an unstructured set of polygons. In such a case, some self-intersections may exist. Nevertheless, it is still possible to construct PLC using a mesh repair technique such as (Zhou et al., 2016).

CDT can be built from a given PLC using the Si’s method (Si, 2006). It results in a tetrahedral mesh, containing two kinds of faces: occlusive faces, belonging to the scene geometry; and some non-occlusive faces, introduced to build the partition. Obviously, a given ray should traverse the latter, as non-occlusive faces do not belong to the input geometry.

2.3 CDT traversal

Finding the closest intersection between a ray and CDT geometry is done in two main steps. First, the

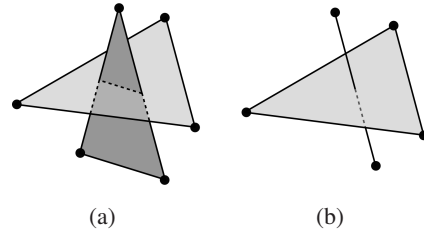


Figure 2: Examples of two non-PLC configurations: intersection between (a) two faces, (b) an edge and a face.

tetrahedron containing the ray origin is located. Second, the ray goes through the tetrahedralization by traversing one tetrahedron at a time until hitting an occlusive face. This process is illustrated in Figure 3. Let us notice that there is no need to explicitly test intersections with the scene geometry, as usual acceleration structures do. This is done implicitly by searching the exit face from inside a tetrahedron.

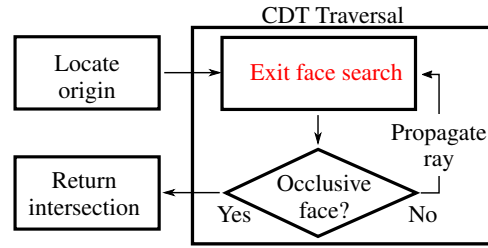


Figure 3: CDT traversal overview: the main key of any CDT traversal algorithm lies in the “exit face search” part.

2.3.1 Locating ray origin

Using pinhole camera model, all primary rays start from the same origin. For an interactive application locating this origin is needed only for the first frame, hence it is a negligible problem. Indeed, camera motion generally corresponds to a translation, for instance when the camera is shifted, or when ray origins are locally perturbed for depth-of-field effect. Using a maximal distance in the traversal algorithm efficiently solves this kind of move.

Locating the origin of non primary rays is avoided by exploiting implicit ray connectivity inside CDT: both starting point and volume correspond to the arrival of the previous ray.

2.3.2 Exit face search

Several methods have been proposed in order to find the exit face of a ray from inside a tetrahedron. (Lagae and Dutré, 2008) present four different ones. The first uses four ray/plane intersections and is similar to

(Garrity, 1990). The second is based on half space classification. The third finds the exit face using 6 permuted inner products (called side and noted \odot) of Plücker coordinates (Shoemake, 1998). It is similar to (Platis and Theoharis, 2003) technique. Their fourth and fastest method uses 3 to 6 Scalar Triple Products (STP). It is remarkable that none of these four methods exploits the knowledge of the ray entry face.

For volume rendering, (Marmitt and Slusallek, 2006) extend (Platis and Theoharis, 2003). Their method (from now MS06) exploits neighborhood relations between tetrahedra to automatically discard the entry face. It finds the exit face using 2,67 side products on average. Since the number of products varies, MS06 exhibits some thread divergence in parallel environment. This drawback also appears with the fastest Lagae *et al.* method.

All these methods are not directly usable on GPU, due to numerical instability. Indeed, the insufficient arithmetic precision with 32-bits floats causes some failures to traverse CDT, leading to infinite loops.

In this paper, we propose a new traversal algorithm, based on Plücker coordinates. Like MS06, it exploits the neighborhood relations between faces. The originality lies in our specific tetrahedron representation, allowing to use exactly 2 optimized side products.

3 NEW TRAVERSAL ALGORITHM

CDT traversal algorithm is a loop, searching for the exit face from inside a tetrahedron (Figure 3). We propose a new algorithm, both fast and robust. It uses Plücker coordinates, *i.e.* six coordinates corresponding to the line direction u and moment v . Such a line is oriented: it passes through a first point p , and then a second one q . Then, $u = q - p$ and $v = p \times q$. For two lines $l = \{u : v\}$ and $l' = \{u' : v'\}$, the sign of the side product $l \odot l' = u \cdot v' + v \cdot u'$ indicates the relative orientation of the two lines: negative value means clockwise orientation, zero value indicates intersection, and positive value signifies counterclockwise orientation (Shoemake, 1998).

3.1 Exit face search

Our algorithm assumes that the entry face is known, and that the ray stabs the current tetrahedron. For a given entry face, we use its complement in the tetrahedron, *i.e.* the part made of one vertex, three edges and three faces. We denote Λ_0 , Λ_1 and Λ_2 the complement edges, with counterclockwise orientation from inside

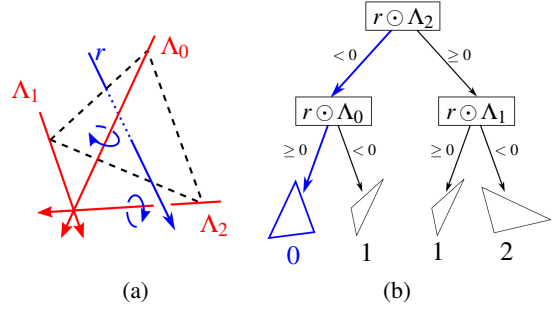


Figure 4: Exit face search example: (a) ray r enters the tetrahedron through the back face; (b) $r \odot \Lambda_2 < 0$ and $r \odot \Lambda_0 \geq 0$, so the exit face is identified by 0.

the tetrahedron (Figure 4). We number complement faces with a local identifier from 0 to 2, such that: face 0 is bounded by Λ_0 and Λ_2 , face 1 is bounded by Λ_1 and Λ_0 , and face 2 is bounded by Λ_2 and Λ_1 . Using Plücker side product, the face stabbed by ray r is:

- face 0, if and only if r turns counterclockwise around Λ_0 and clockwise around Λ_2 ($r \odot \Lambda_0 \geq 0$ and $r \odot \Lambda_2 < 0$);
- face 1, if and only if r turns counterclockwise around Λ_1 and clockwise around Λ_0 ($r \odot \Lambda_1 \geq 0$ and $r \odot \Lambda_0 < 0$);
- face 2, if and only if r turns counterclockwise around Λ_2 and clockwise around Λ_1 ($r \odot \Lambda_2 \geq 0$ and $r \odot \Lambda_1 < 0$).

We compact these conditions into a decision tree (Figure 4(b)). Each leaf corresponds to an exit face, and each interior node represents a side product between r and a line Λ_i . At the root, we check $r \odot \Lambda_2$. If it is negative (clockwise), then r cannot stab face 2: in the left subtree, we only have to determine if r stabs face 0 or 1, using their shared edge Λ_0 . Otherwise, r turns counterclockwise around Λ_2 and so cannot stab face 0, and the right subtree we check if r stabs face 1 or 2 using their shared edge Λ_1 . With Figure 4(a) example, r turns clockwise around Λ_2 and then counterclockwise around Λ_0 ; so, r exits through face 0.

Require: $F_e = \{\Lambda_0, \Lambda_1, \Lambda_2\}$: entry face; Λ_r : ray;

Ensure: F_s : exit face;

- 1: $side \leftarrow \Lambda_r \odot F_e \cdot \Lambda_2$;
- 2: $id \leftarrow (side \geq 0); \{id \in \{0, 1\}\}$
- 3: $side \leftarrow \Lambda_r \odot F_e \cdot \Lambda_{id}$;
- 4: $id \leftarrow id + (side < 0); \{id \in \{0, 1, 2\}\}$
- 5: $F_s \leftarrow \text{getFace}(F_e, id)$;
- 6: **return** F_s ;

Algorithm 1: Exit face search from inside a tetrahedron.

Exit identifier	Entry face			
	F_0	F_1	F_2	F_3
0	F_1	F_0	F_0	F_0
1	F_2	F_3	F_1	F_2
2	F_3	F_2	F_3	F_1

Table 1: Exit face according to the entry face and a local identifier in $\{0, 1, 2\}$, following a consistent face numbering (Figure 5(a)).

Since every decision tree branch has a fixed depth of 2, our new exit face search method answers using exactly two side products. Moreover, it is optimized to run efficiently without any conditional instruction (Algorithm 1). Notice that leave labels form two pairs from left to right: the first pair (0,1) is equal to the second (1,2), minus 1. Then, it uses that successful logical test returns 1 (and 0 in failure case) to decide which face to discard. So, the test $r \odot \Lambda_2 \geq 0$ allows to decide if we have to consider the first or the second pair. Finally, the same method is used with either the line Λ_0 or Λ_1 .

This algorithm ends with `getFace` function call. This function returns the tetrahedron face number according to the entry face and to the exit face label. It answers using a lookup-table, defined using simple combinatorics (Table 1), assuming a consistent labeling of tetrahedron faces (Figure 5(a)).

3.2 Data structure

Algorithm 1 works for any entry face of any tetrahedron. It relies on two specific representations of the tetrahedron faces: a local identifier in $\{0, 1, 2\}$, and global face F_i , $i \in [0 \dots 3]$. For a given face, it uses 3 Plücker lines Λ_i . Since such lines contain 6 coordinates, a face needs 18 single precision floats for the lines (18×32 bits), plus `brdf` and neighborhood data (tetrahedron and face numbers).

To reduce data size and balance GPU computations and memory accesses, we dynamically calculate the Plücker lines knowing their extremities: each line starts from a face vertex and ends with the complement vertex. So, we need all the tetrahedron vertices. We arrange the faces such that their complement vertex have the same number, implicitly known. Vertices are stored into tetrahedra (for coalescent memory accesses), and vertex indices (in $[0 \dots 3]$) are stored into faces. This leads to the following data structure:

```
struct Face {
  int brdf; // -1: Non-Occlusive
  int tetra; // neighbor
  int face; // neighbor
  int idV[3]; // face vertices
};
```

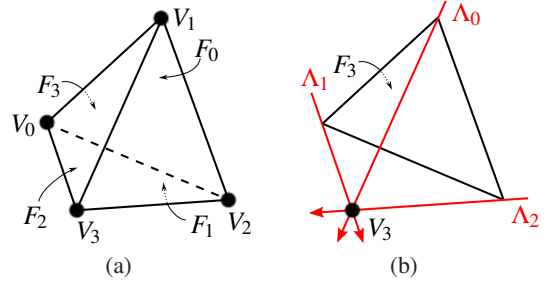


Figure 5: Description of a tetrahedron: (a) vertices and faces numbering; (b) the complement vertex for F_3 is $\{V_3\}$, and its edges are $\Lambda_0 = V_1V_3$, $\Lambda_1 = V_0V_3$ and $\Lambda_2 = V_2V_3$.

```
struct Tetrahedron {
  float3 V[4]; // vertices
  Face F[4]; // faces
};
```

To save memory and so bandwidth, we compact the structure `Face`. The neighboring face (the field face) is a number between 0 and 3; it can be encoded using two bits, and so packed with the field `tetra`, corresponding to the neighboring tetrahedron. Thus, tetrahedron identifiers are encoded on 30 bits, allowing a maximum of one billion tetrahedra. In a similar way, field `idV` needs only 2 bits per vertex. But, they are common to all the tetrahedra, and so are stored only once for all into 4 unsigned `char`. Hence, a face needs 8 bytes, and a full tetrahedron 80 bytes. Notice that, on GPU a vertex is represented by 4 floats to have aligned memory accesses. Then on GPU a full tetrahedron needs 96 bytes.

Figure 5 proposes an example: for F_3 (made using the complement vertex V_3 and counterclockwise vertices V_1, V_0 and V_2), we can deduce that $\Lambda_0 = V_1V_3$, $\Lambda_1 = V_0V_3$ and $\Lambda_2 = V_2V_3$. Table 2 gives the description of faces according to their vertices and edges, following face numbering presented in Figure 5(a).

F	Vertexes	Λ_0	Λ_1	Λ_2
0	$\{3, 1, 2\}$	V_3V_0	V_1V_0	V_2V_0
1	$\{2, 0, 3\}$	V_2V_1	V_0V_1	V_3V_1
2	$\{3, 0, 1\}$	V_3V_2	V_0V_2	V_1V_2
3	$\{1, 0, 2\}$	V_1V_3	V_0V_3	V_2V_3

Table 2: Complement edges of entry face F_i are implicitly described by the face complement vertex (identified by i), and its vertices in counterclockwise order.

3.3 Exiting the starting volume

Algorithm 1 assumes known the entry face. This condition is not fulfilled for the starting tetrahedron. Algorithm 1 must be adapted in that case. A simple solution lies in using a decision tree of depth 4, leading

to three Plücker side products. One can settle this tree starting with any edge to discriminate between two faces, and so on with the children.

Nevertheless, a simpler but equivalent solution exists. Once the root fixed, we have only three possible exit faces. This corresponds to Algorithm 1, as if the discarded face was the entry one. So, we just choose one edge to discard a face and then we call Algorithm 1 with the discarded exit face as the fake entry one. This leads to Algorithm 2. We naturally choose edge V_2V_3 shared by faces F_0 and F_1 (Figure 5(a)). If the side product is negative, then we cannot exit through F_1 . Else, with a positive or null value, we cannot exit through F_0 . Thus, the starting tetrahedron problem is solved using three and only three side products.

Require: $T = \{V_i, F_i\}_{i \in \{0..3\}}$: Tetrahedron; Λ_r : Ray;
Ensure: F_s : exit face;
 1: $side \leftarrow \Lambda_r \odot V_2V_3$;
 2: $f \leftarrow side < 0; \{f \in \{0, 1\}\}$
 3: **return** $ExitTetra(F_f, \Lambda_r); \{\text{Algorithm 1}\}$

Algorithm 2: Exit face search from the starting tetrahedron.

3.4 Efficient side product

Both Algorithm 1 and 2 use Plücker side products. A naive approach results in 23 operations per side product: to calculate Plücker coordinates, we need 3 subtractions for its direction and 6 multiplications and 3 subtractions for its moment. Then, side product needs 6 multiplications and 5 additions. The two side products in Algorithm 1 result in 46 operations.

We propose a new method using less operations. It rests upon a coordinate system translation to the complement vertex V_f of the entry face. In this local system, lines Λ_i have a nil moment (since they contain the origin). So, side products are inner products of vectors having only 3 coordinates: each one needs 3 multiplications and 2 additions. Moreover, line directions are computed using 3 subtractions. Hence, such side products need only 8 operations.

Nevertheless, we also need to modify Plücker coordinates of the ray r to obtain valid side products. Let us recall how a Plücker line is made. We compute its direction u using two points p and q on the line, and its moment v with $p \times q = p \times u$. In the local coordinates system, the new line coordinates must be calculated using translated points. The direction is

obviously the same, only v is modified:

$$\begin{aligned} v' &= (p - V_f) \times u \\ &= p \times u - V_f \times u \\ &= v - V_f \times u. \end{aligned}$$

So, v' is calculated using 12 operations: 3 subtractions, 6 multiplications and 3 subtractions. This ray transformation is done once per tetrahedron, the local coordinates system being shared for all the lines Λ_i .

As a conclusion, the number of arithmetic operations involved in Algorithm 1 can be decreased from 46 to 28, saving about 40% of computations.

4 EXPERIMENTS

This section discusses some experiments made using our new traversal algorithm.

4.1 Results

Performance is evaluated using three objects tetrahedralized using Tetgen (Si, 2015). Table 3 sums up their main characteristics and measured performance. The simplest object is constructed from a banana model, with 25k occlusive faces. The other two correspond to well-known Stanford’s objects: BUNNY and ARMADILLO. Their CDT respectively count 200k and 1.1M occlusive faces. We use quality CDT, introducing new vertices into object models, explaining the high number of faces our three objects have.

Performance is measured in millions of ray cast per second (Mrays/s) using ray casting, 1024×1024 pixels and no anti-aliasing. The used computer possesses an Intel® Core™ i7-4930K CPU @ 3.40Ghz, 32 Gb RAM and NVidia® GeForce® GTX 680. Algorithms are made parallel on CPU (OpenMP) and GPU (CUDA, with persistent threads (Aila et al., 2012)). On average, CPU ray casting reaches 9 Mrays/s, GPU version 280 Mrays/s.

4.2 Traversal

Closest ray/object intersection is found by traversing CDT one tetrahedron at a time until hitting an occlusive face. The ray traversal complexity is linear in the number of traversed tetrahedra. Figure 6 shows the relation between execution time (T) and number of traversed tetrahedra per image (Φ). Statistics are extracted on CPU using 1,282 points of view from BUNNY. The execution time is proportional to Φ : on point of view (A), almost 10 millions tetrahedra are traversed in 40.1 ms; on point of view (B), we traverse 23 millions tetrahedra in 122 ms. It is

		BANANA	BUNNY	ARMADILLO
				
Tetrahedra		71,300	682,733	2,990,552
Occlusive faces		24,568	222,775	1,105,218
Non-occlusive faces		117,994	1,142,650	4,875,834
Memory (MB)		6	62	273
Ray-casting (Mray/s)	CPU	9.76	10.5	6.75
	GPU	428	289	123

Table 3: Scenes characteristics and performance: number of tetrahedra, number of occlusive faces (faces coming from the model), number of non-occlusive faces (faces created during tetrahedralization), occupied memory and ray casting performance in millions of ray cast per second on CPU and GPU.

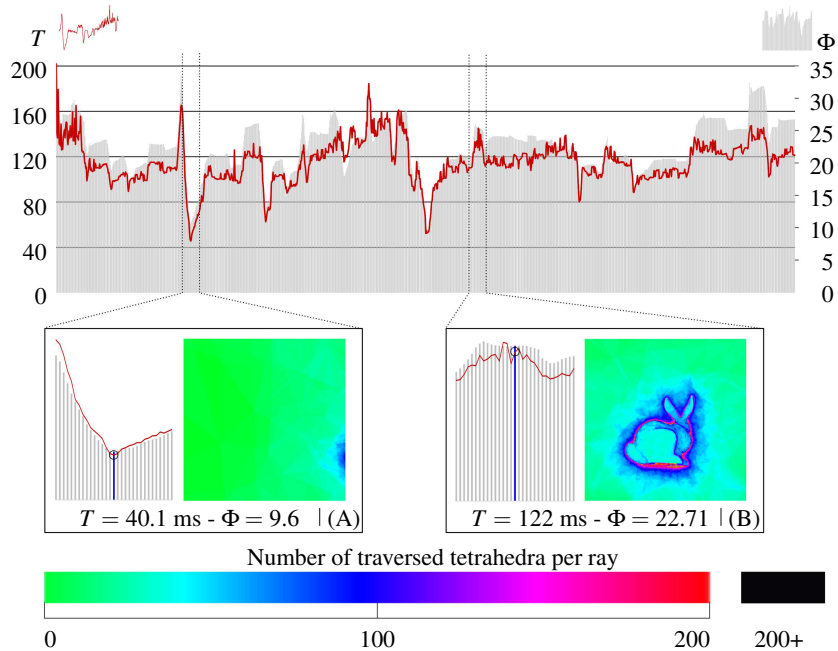


Figure 6: Rendering times on CPU in ms (T , red curve) and number of traversed tetrahedra in millions (Φ , gray bars) using 1,282 points of view and BUNNY; (A) $T = 40.1$ ms - $\Phi = 9.6$; (B) $T = 122$ ms - $\Phi = 22.71$.

not strictly proportional, mainly due to memory accesses that become more important when more tetrahedra are traversed, leading to more memory cache defaults. False-colored image of point of view (B) reveals that rays going close to object boundary traverse more tetrahedra.

4.3 Numerical robustness

Using floating-point numbers can cause errors due to numerical instability. Tetgen uses geometric predicates (*e.g.* (Shewchuk, 1996) or (Devillers and Pion, 2003)) to construct robust CDT. If this is common practice in algebraic geometry, it is not the case in

rendering. Hence, it is too expensive to be used in CDT ray traversal.

We experimented three methods proposed in (Lagae and Dutré, 2008) (ray/plane intersection tests, Plücker coordinates and STP), plus the method proposed in (Marmitt and Slusallek, 2006) (MS06) (Section 2.3.2). We noticed they all suffer from numerical errors either on CPU or GPU. Indeed, calculations are not enough precise with rather flat tetrahedra. Thus, without extra treatment (like moving the vertices) these algorithms may return a wrong exit face or do not find any face at all (no test is valid). Table 4 reports for each object the number of rays per image concerned by this problem, averaged over points of

	BANANA	BUNNY	ARMADILLO
Ray/plane	33.27	40.85	74.85
Plücker	3.6	22.25	412.13
STP	63.07	204.89	456.65
MS06	0.0007	0.004	0.422
Ours	0	0	0

Table 4: Numerical errors impact on GPU: number of rays suffering from wrong results for 1024×1024 pixels, and averaged over about 1,300 points of view.

view series.

In contrast, we did not obtain wrong results using our method. It can be explained by the smaller number of performed arithmetic operations; less numerical errors accumulated, more accurate results.

4.4 Exit face search comparison

This section compares performance of our exit face search algorithm with the same 4 previous methods: ray/plane intersection tests, Plücker coordinates, STP and MS06 (Section 2.3.2). Statistics are summed up in Table 5. Times are measured for 16,384 random rays stabbing 10,000 random tetrahedra, both on CPU (using one thread) and GPU.

Method	Time (ms)	
	CPU	GPU
Ray/plane	15,623	36
Plücker	10,101	28
STP	4,876	29
MS06	5,994	21
Ours	2,663	13

Table 5: Exit face search comparison: time (in ms) to determine the exit face for 10,000 tetrahedra and 16,384 random rays per tetrahedron; on CPU (single thread) and on GPU.

CPU results show that our method is much more efficient than former ones. This behavior is expected since our new method requires less arithmetic operations. STP is the fastest previous method, but is 83% slower than ours.

On GPU, results are slightly different. For example, Plücker method is faster than STP. Indeed, even if it requires more operations, it does not add extra thread divergence. Hence, it is more adapted to GPU. Among the previous GPU methods, the most efficient is MS06, still 59% slower than ours.

4.5 State-of-the-art comparison

In (Lagae and Dutré, 2008), authors noticed that rendering using CDT as acceleration structure takes two to three more computation times than using kd-tree. In

	CDT	BVH (Aila et al., 2012)
BANANA	315-947	200-260
BUNNY	130-1040	160-260
ARMADILLO	82-160	130-260

Table 6: Performance comparison with (Aila et al., 2012), in number of frames per second.

this last section, we check if it is still the case using our new tetrahedron exit algorithm and on GPU. We compare our GPU ray-tracer with the state-of-the-art ray tracer (Aila et al., 2012), always using the same computer. Their acceleration structure is BVH, constructed using SAH (MacDonald and Booth, 1990) and split of large triangles (Ernst and Greiner, 2007). To our knowledge, nowadays their implementation is the fastest GPU one.

Table 6 sums up this comparison. Results show that CDT is still not a faster acceleration structure than classical ones (at least than BVH on GPU). First, the timings show larger amplitude using CDT than BVH. Moreover, while CDT is on average faster than BVH with BANANA and BUNNY models, it is no more true using ARMADILLO. This is directly linked to the traversal complexity of the two structures. BVH being built up following SAH, its performance is less impacted with the geometry input size, contrary to CDT where this size has a direct impact on performance. Clearly, a heuristics similar to SAH is missing for tetrahedralization.

5 CONCLUSION

This article proposes a new CDT ray traversal algorithm. It is based upon a specific tetrahedron representation, and fast Plücker side products. It uses less arithmetic operations than previous methods. Last but not least, it does not involve any conditional instructions, employing two and only two side products to exit a given tetrahedron.

This algorithm exhibits several advantages compared to the previous ones. Firstly it is inherently faster, requiring less arithmetic operations. Secondly it is more adapted to parallel computing, since having a fixed number of operations it does not involve extra thread divergence. Finally, it is robust and works with 32-bits floats either on CPU or GPU.

As future work, we plan to design a new construction heuristic, to obtain as fast to traverse as possible CDT. Indeed, CDT traversal speed highly depends on its construction. CDT traversal complexity is linear in the number of traversed tetrahedra: the less tra-

versed tetrahedra, the more high performance. Before SAH introduction, the same problem existed with well-known acceleration structures like kd-tree and BVH, for which performance highly depends on the geometric model. Since CDT for ray-tracing is a recent method, we expect that similar heuristics exists.

REFERENCES

- Aila, T. and Laine, S. (2009). Understanding the Efficiency of Ray Traversal on GPUs. In *High-Performance Graphics*, HPG '09, pages 145–149.
- Aila, T., Laine, S., and Karras, T. (2012). Understanding the efficiency of ray traversal on GPUs – Kepler and Fermi addendum. Technical report, NVIDIA Corp.
- Bentley, J. L. (1975). Multidimensional Binary Search Trees Used for Associative Searching. *Communications of the ACM*, 18(9):509–517.
- Chew, L. P. (1989). Constrained Delaunay triangulations. *Algorithmica*, 4:97–108.
- Delaunay, B. (1934). Sur la sphère vide. À la mémoire de Georges Voronoï. *Bulletin de l'Académie des Sciences de l'URSS*, (6):793–800.
- Devillers, O. and Pion, S. (2003). Efficient Exact Geometric Predicates for Delaunay Triangulations. In *5th Workshop on Algorithm Engineering and Experiments*, ALENEX '03, pages 37–44.
- Edelsbrunner, H. and Tan, T. S. (1992). An upper bound for conforming delaunay triangulations. In *8th Annual Symposium on Computational Geometry*, SCG '92, pages 53–62.
- Ernst, M. and Greiner, G. (2007). Early Split Clipping for Bounding Volume Hierarchies. In *IEEE Symposium on Interactive Ray Tracing*, RT '07, pages 73–78.
- Foley, T. and Sugerma, J. (2005). KD-tree Acceleration Structures for a GPU Raytracer. In *ACM SIGGRAPH/EUROGRAPHICS conference on Graphics Hardware*, HWWS '05, pages 15–22.
- Fortune, S. (1999). Topological Beam Tracing. In *15th Annual Symposium on Computational Geometry*, SCG '99, pages 59–68.
- Fujimoto, A., Tanaka, T., and Iwata, K. (1986). ARTS: Accelerated Ray-Tracing System. *IEEE Computer Graphics and Applications*, 6(4):16–26.
- Garrity, M. P. (1990). Raytracing Irregular Volume Data. *ACM SIGGRAPH Computer Graphics*, 24(5):35–40.
- Günther, J., Popov, S., Seidel, H.-P., and Slusallek, P. (2007). Realtime Ray Tracing on GPU with BVH-based Packet Traversal. In *IEEE Symposium on Interactive Ray Tracing 2007*, RT '07, pages 113–118.
- Havran, V. (2000). *Heuristic Ray Shooting Algorithms*. PhD thesis, Department of Computer Science and Engineering, Faculty of Electrical Engineering, Czech Technical University in Prague.
- Kalojanov, J., Billeter, M., and Slusallek, P. (2011). Two-Level Grids for Ray Tracing on GPUs. *Computer Graphics Forum*, 30(2):307–314.
- Kay, T. L. and Kajiya, J. T. (1986). Ray Tracing Complex Scenes. *ACM SIGGRAPH Computer Graphics*, 20(4):269–278.
- Lagae, A. and Dutré, P. (2008). Accelerating Ray Tracing using Constrained Tetrahedralizations. *Computer Graphics Forum*, (4):1303–1312.
- MacDonald, D. J. and Booth, K. S. (1990). Heuristics for Ray Tracing Using Space Subdivision. *The Visual Computer*, 6(3):153–166.
- Mahovsky, J. and Wyvill, B. (2006). Memory-Conserving Bounding Volume Hierarchies with Coherent Raytracing. *Computer Graphics Forum*, 25(2):173–182.
- Maria, M., Horna, S., and Aveneau, L. (2017). Constrained Convex Space Partition for Ray Tracing in Architectural Environments. *Computer Graphics Forum*.
- Marmitt, G. and Slusallek, P. (2006). Fast Ray Traversal of Tetrahedral and Hexahedral Meshes for Direct Volume Rendering. In *8th Joint EG/IEEE VGTC Conference on Visualization*, EUROVIS '06, pages 235–242.
- Miller, G. L., Talmor, D., Teng, S.-H., Walkington, N., and Wang, H. (1996). Control Volume Meshes using Sphere Packing: Generation, Refinement and Coarsening. In *5th International Meshing Roundtable*, IMR '96, pages 47–62.
- Platis, N. and Theoharis, T. (2003). Fast Ray-Tetrahedron Intersection Using Plucker Coordinates. *Journal of Graphics Tools*, 8(4):37–48.
- Purcell, T. J., Buck, I., Mark, W. R., and Hanrahan, P. (2002). Ray Tracing on Programmable Graphics Hardware. *ACM Transactions on Graphics*, 21(3):703–712.
- Reshetov, A., Soupikov, A., and Hurley, J. (2005). Multi-level Ray Tracing Algorithm. *ACM Transactions on Graphics*, 24(3):1176–1185.
- Rubin, S. M. and Whitted, T. (1980). A 3-dimensional representation for fast rendering of complex scenes. *ACM SIGGRAPH Computer Graphics*, 14(3):110–116.
- Shewchuk, J. R. (1996). Adaptive precision floating-point arithmetic and fast robust geometric predicates. *Discrete & Computational Geometry*, 18:305–363.
- Shewchuk, J. R. (1998). Tetrahedral Mesh Generation by Delaunay Refinement. In *14th Annual Symposium on Computational Geometry*, SCG '98, pages 86–95.
- Shoemake, K. (1998). Plücker coordinate tutorial. *Ray Tracing News*, 11:20–25.
- Si, H. (2006). On Refinement of Constrained Delaunay Tetrahedralizations. In *15th International Meshing Roundtable*, IMR '06, pages 509–528.
- Si, H. (2015). TetGen, a Delaunay-Based Quality Tetrahedral Mesh Generator. *ACM Transactions on Mathematical Software*, 41(2).
- Wald, I., Slusallek, P., Benthin, C., and Wagner, M. (2001). Interactive Rendering with Coherent Ray Tracing. *Computer Graphics Forum*, 20(3):153–165.
- Zhou, Q., Grinspun, E., Zorin, D., and Jacobson, A. (2016). Mesh Arrangements for Solid Geometry. *ACM Transactions on Graphics*, 35(4).